




Clinical implementation of a rotating pod for lung tumor in fixed ion beamlines

Jia-Yao Sun^{1,2,3} · Wen-Xuan Yang^{1,2,3} · Ya-Qi Li^{2,3,4} · Jian Chen^{2,3,5} · Jing-Fang Mao^{2,3,5} · Ning-Yi Ma^{2,3,5} · Yin-Xiang-Zi Sheng^{1,2,3} · Wei-Wei Wang^{1,2,3} · Dan You^{1,2,3} · Kai-Liang Wu^{2,3,5} 

Received: 18 April 2024 / Revised: 26 May 2024 / Accepted: 2 July 2024 / Published online: 8 May 2025

© The Author(s), under exclusive licence to China Science Publishing & Media Ltd. (Science Press), Shanghai Institute of Applied Physics, the Chinese Academy of Sciences, Chinese Nuclear Society 2025

Abstract

The purpose of this study was to evaluate the clinical application of a rotating pod and assess its dosimetric considerations, positional accuracy, and anatomical structure stability. A pre-dosimetric study conducted on 11 patients revealed the potential for lung dose reduction using the rotational pod. Subsequently, seven patients underwent treatment with the rotational pod, and the target coverage and organs at risk doses were compared with those of conventional methods. The positional accuracy of the rotational pod, in collaboration with the imaging guidance system, was analyzed. The Dice similarity coefficient (DSC) was used to assess the settlement of tumors, trachea, and thoracic vertebrae after rotation for 20 min. In the pre-dosimetric study, there was no statistically significant difference in the volume of the internal gross tumor volume receiving $\geq 99\%$ of the prescription dose between the pod and conventional couch plans. However, compared to conventional couch plans, pod plans demonstrated a significant reduction in the average lung dose by 5 – 53% ($p < 0.01$). Patient accrual, comprising seven cases, revealed reduced lung doses (9 – 26%) in four patients. For the other three patients, although there was no significant reduction in the lung dose, the use of the 90° beamline contributed to a decrease in the patient admission waiting time. The positional errors between the beams for lateral, longitudinal, vertical, ISO, pitch, and roll directions were $0.0 \text{ mm} \pm 5.3 \text{ mm}$, $-1.2 \text{ mm} \pm 2.3 \text{ mm}$, $-1.1 \text{ mm} \pm 2.7 \text{ mm}$, $0.0^\circ \pm 0.6^\circ$, $-0.1^\circ \pm 0.5^\circ$, and $0.0^\circ \pm 0.8^\circ$, respectively. The DSC for the target region and thoracic vertebrae between CT images captured before and after a 20-min rotation was higher than 0.85, whereas the DSC for the trachea was approximately 0.8. The preliminary clinical application of the rotational pod for lung tumors in fixed ion beamlines shows promise for achieving target coverage, reducing lung dose, and maintaining position accuracy.

Keywords Rotational pod · Carbon-ion radiotherapy · Lung cancer · Position accuracy

1 Introduction

A well-optimized plan for ion radiotherapy can frequently be attained using no more than four beam-entry angles achieved through the rotation of the gantry, rotation of the patient positioning table, or a combination of both. The selection of these angles is pivotal for achieving the prescribed target

J. Sun and W. Yang have contributed equally to this work.

This work was supported by the Shanghai Municipal Health Commission Funds (No. 20214Y0026).

✉ Kai-Liang Wu
wukailiang@aliyun.com

¹ Department of Medical Physics, Shanghai Proton and Heavy Ion Center, Fudan University Cancer Hospital, Shanghai 201321, China

² Shanghai Engineering Research Center of Proton and Heavy Ion Radiation Therapy, Shanghai 201321, China

³ Shanghai Key Laboratory of Radiation Oncology, Shanghai 201321, China

⁴ Department of Radiation Oncology, Shanghai Proton and Heavy Ion Center, Shanghai 201321, China

⁵ Department of Radiation Oncology, Shanghai Proton and Heavy Ion Center, Fudan University Cancer Hospital, Shanghai 201321, China

dose while minimizing the dose to the organs at risk (OARs) [1, 2]. However, the practical implementation of a carbon-ion rotational gantry is challenging, with dimensions and weight double those of proton gantries, currently limited to institutions in Germany and Japan [3–7]. With the advancement of superconducting magnet technology, the first superconducting carbon-ion gantry was installed at the National Institutes for quantum science and technology (QST), which reduced the weight of the gantry at the Heidelberg ion beam therapy center (HIT) from 600 to 300 tons [5]. Toshiba has increased the superconducting magnetic field strength to 3.50 T to develop a more compact carbon-ion gantry. This gantry is currently in the commissioning phase at Yamagata University and Yonsei University Health System. The size of the system has been reduced to two-thirds that of the first superconducting gantry in QST [8]. Radiation protection in carbon-ion radiotherapy is crucial because of the necessity for high-energy therapeutic carbon-ion beams for treating deep-seated tumors [9–12]. This importance is amplified when considering the rotating gantry for carbon-ion therapy. Given the substantial size and cost of carbon-ion rotational gantries, Shanghai proton and heavy ion center (SPHIC), as most institutions globally, has not yet adopted this technology [13]. SPHIC currently operates four proton and heavy ion therapy rooms, catering to diverse tumor locations, depths, and positioning requirements, including three horizontal beamline treatment rooms and one 45° beamline treatment room.

Carbon-ion radiotherapy, distinguished by its superior physical dosimetry compared to that of conventional radiation and augmented by the biological advantages of carbon-ion beams, holds promise for better preservation of healthy tissue and increased tumor control [14]. Consequently, it has been increasingly employed in the treatment of patients with compromised pulmonary or cardiac function [15–17]. Given the significant correlation between the mean lung dose and risk of radiation pneumonitis, it is imperative to minimize the mean lung dose [18, 19]. The selection of appropriate beam angles is crucial in achieving this objective [20]. Because particle therapy typically involves fewer beam-entry angles than that of conventional radiation, providing freedom in selecting beam angles is crucial from a hardware standpoint.

Usage challenges arise because the fixed-angle beamline and limited roll rotation of the treatment couch hinder optimal treatment for certain patients. In addition, the 45° beamline treatment room faces significant patient waiting times, impacting subsequent treatment processes. Recently, a six-degree-of-freedom treatment chair (6DTC) was designed and installed at our center [2, 21]. However, limited by the absence of an upright CT, the 6DTC can only treat patients with head and neck cancers [1, 22]. To address constraints in treating lung and abdominal tumors, a clinical solution has

been developed: a rotational pod. This pod enables patients to be fixed and rotated by 360 degrees (180 clockwise and 180 counterclockwise), simulating the effect of a rotational gantry, thereby ensuring the necessary beam angles and desired dose distribution.

The concept of treatment pods, pioneered by the Paul Scherrer Institute in Switzerland [23], utilizes pi-meson beams directed at tumors through magnets, allowing three-dimensional movement of patients during treatment. Loma Linda University in the USA employs advanced technology [24], utilizing a white semi-cylindrical pod filled with a liquid polyurethane mixture that expands into a solid foam for personalized fixation. In Japan, QST incorporates respiratory gating technology into a rotational pod [25], enabling ± 20 -degree rotation. The University of Sydney integrates an Elekta linear accelerator and a Patient Rotational System [26] to achieve submillimeter accuracy.

Despite these advances, there is currently a paucity of literature providing detailed clinical data on patients treated with pods. This study aims to fill this gap by presenting comprehensive clinical trial data from patients treated with rotational pods at our center. Specifically, this study aims to investigate the dosimetric benefits of the increased flexibility of beam-angle selection provided by pods for lung cancer patients through pre-dosimetry analysis. Additionally, it will validate the dosimetric advantages by examining clinical treatment data from pod patients. The positional accuracy of the pods and the impact of settlement on the stability of tumors and OARs are also calculated and evaluated.

2 Materials and methods

2.1 Structure of the pod

The rotational pod comprises four key components: the pod body, pod cover, rotation device, and connectors, as depicted in Fig. 1. Patients can recline inside the rotating treatment pod using a staircase and handrails. The rotating treatment pod can then be transported using a transfer cart and maneuvered into the CT positioning room or treatment room, connecting it with the current clinical 6-DOF robotic arm via connectors. The rotational robotic arm allows for the necessary adjustments and displacements of the rotating pod within the treatment space, thereby minimizing collisions with other preexisting equipment in the treatment room. The rotation device enables 360-degree roll rotation of the pod body and features a locking mechanism. The pod cover facilitates patient entry and closes securely when the patient remains inside. A specifically designed facial opening in the pod cover ensures that the patient's face is fully exposed, thereby fostering improved communication with

Fig. 1 Color online **a** Structure of the pod. **b** Stairs and the handrails for entering the pod. **c** Individualized low-density foam cradle. **d** CT planning procedure. **e** Position verification procedure. **f** Beam-on procedure. The pod rotation angle is 30° for figures d and e, and 40° for figure f



the physicians and therapists upon entering the rotating treatment pod.

2.2 Pre-dosimetry study

Before initiating the clinical trial, a preliminary dosimetry study was conducted to identify suitable indications for pod use. The average lung dose is a critical OAR in lung cancer radiotherapy. Typically, selecting a path that traverses the shortest distance through the lungs can minimize the average lung dose [27]. However, our facility is constrained to beamlines with angles of 90 and 45 degrees, which limits the options for the beam-entry directions. The application of a pod introduces greater flexibility in the selection of entry angles. In this study, 11 patients who demonstrated a reduced path through the lung when the couch was rotated at a certain angle were selected from those who had previously undergone carbon-ion radiotherapy at our center. The patients' CT scans and structures were imported into

custom-made software and rotated using a rigid transformation method to the angle at which the beam path through the lung was minimized, creating a synthetic CT. The pod simulation plans were optimized using the same prescription and dose limits as those for the treatment plans with the conventional treatment couch. Then, the target coverage and dose to the OARs were compared between the couch-based and pod simulation plans.

2.3 Immobilization and CT simulation

During multidisciplinary team (MDT) discussions, physicians and physicists assess whether a patient is potentially suitable for rotational pod treatment based on factors such as tumor location, surrounding normal tissue structures, beam path, and other comprehensive considerations. The treatment angles for the rotational pod are determined based on imaging data. After the MDT discussion, patients undergo immobilization following respiratory training [15, 28]. A

low-density foam cradle secures the patient's back, utilizing a thermoplastic mask for fixation when the pod rotation angle is $\leq 30^\circ$ and employing a pod cover with foam filling when the angle exceeds 30° . Following a supine 4DCT scan, the pod is rotated to the treatment angle for another CT scan [29]. The parameters of both CT scans are identical. The slice thickness is set to 3 mm. A subsequent scan is performed after 20 min at the treatment angle. During this 20-min interval, the patient remains at the treatment angle, simulating the actual treatment. A respiratory gating system (AZ-733V, Anzai Medical, Japan) was used to mitigate the effects of respiratory motion [30].

2.4 Treatment planning

For each patient, two sets of plans were devised: one utilizing supine CT, and the other incorporating CT with a rotated pod. The treatment plan for the supine CT (hereafter referred to as the supine plan) can employ either a 90-degree or 45-degree beamline. Given that the key objective of the pod development is to alleviate the high occupancy pressure associated with the 45° beamline, the pod plan prioritizes the use of a 90-degree beamline. Depending on the different stages and types of tumors in the patients, different prescriptions of carbon-ion irradiation were administered. The relative biological effectiveness (RBE) was calculated using local effect model I [31]. The planning objectives aimed to ensure that at least 95% of the internal gross tumor volume (iGTV) and clinical target volume (CTV) received 99% of the prescription dose while minimizing the OAR dose with no more than four beams. If the dose to the normal lung exceeds the limit, the target coverage is sacrificed [29]. Owing to the absence of a robust planning technique [32] in Syngo (V13, Siemens, Germany), the planning target volume (PTV) was expanded based on plan-specific

factors, such as the chosen beam range uncertainty, ranging from 7–15 mm [33, 34]. Patients deemed to require two pod rotation angles during the MDT discussions were immobilized and scanned at both angles. Subsequently, the treatment plans were devised separately based on the respective CT scans. Deformable dose accumulation was performed to assess the total dose to the target and OARs using MIM (MIM Software, Cleveland, OH, USA). All plans were reviewed by the chief physician. A comparison was made between the target coverage and OAR doses of the two plan types.

Patients were considered eligible for pod treatment based on three criteria: lower OAR dose, comparable target coverage, and no increase in range uncertainty. In cases where both plans demonstrated similar target coverage, OAR doses, and uncertainties, the pod plan was preferred because of its shorter admission waiting time, aligning with the best interests of the patients.

Seven patients were selected to undergo carbon-ion radiotherapy using a pod based on the aforementioned criteria. The characteristics of these seven patients' are shown in Table 1.

2.5 Alignment and treatment

The treatment procedure was based on the 6DTC treatment protocol established at our center [1]. During the initial fraction of treatment, an in-room CT scan was conducted to ensure minimal tumor or anatomical changes compared to the planning CT scan at the treatment angle. If the CT results were satisfactory, the pod was repositioned to the first treatment angle using the robotic arms. Repositioning of patients or adaptive planning was initiated when anatomical changes occurred between the review and planning CTs [33]. The position was verified using an image-guided radiation

Table 1 Patient information

Patient	1	2	3	4	5	6	7
Age	58	69	54	41	64	48	67
Gender	M	M	M	F	M	M	M
Weight (kg)	69	56	76	79	63	89	59
Height (cm)	169	172	173	168	174	165	168
KPS	90	90	90	90	90	90	90
Disease ^a	NSCLC	LUAD	LSCC	M-MPNST	LSCC	LSCC	LSCC
Prescription [Gy(RBE)]	72/16	65/10	77/22	70.4/16	77/22	77/22	77/22
Ion species	Carbon ion	Carbon ion	Carbon ion	Carbon ion	Carbon ion	Carbon ion	Carbon ion
Pod rotation angle (°)	25	45	45	45+90 ^b	45	35 + 40 ^c	30

^a Abbreviations: NSCLC, non-small cell lung cancer; LUAD, lung adenocarcinoma; LSCC, lung squamous cell carcinoma; and M-MPNST, mediastinal malignant peripheral nerve sheath tumor

^b This patient underwent treatment with a 45° rotation for seven fractions and a 90° rotation for nine fractions

^c This patient underwent treatment with a rotation counterclockwise 35° for 11 fractions and a clockwise 40° rotation for 11 fractions

therapy (IGRT) system. A set of orthogonal X-ray images was captured and registered with digitally reconstructed radiographs, focusing on the bony anatomy. The positional errors at the initial beam position (PE-B1) were documented, including three translational shifts (lateral, longitudinal, and vertical) and three rotational shifts (iso, pitch, and roll) [1]. Subsequently, the patient's position was adjusted using PE-B1 followed by beam delivery. Upon completion of the first beam delivery, the pod was moved to the second isorotation angle. The X-ray alignment procedure was repeated to determine the positional errors in the second beam position (PE-B2). After applying PE-B2, a second beam was delivered. This process was repeated if the treatment fraction involves more than two beams. The attending physician assessed and authorized the alignment before each treatment onsite.

2.6 Position accuracy analysis

In the treatment of lung cancer patients using the pod, maintaining stability in anatomical structures such as the trachea, thoracic vertebrae, and tumor at the treatment angle is paramount, given the inclined position of the body within the pod. This study conducted a comparative analysis of the anatomical structural stability based on CT images acquired 20 min apart. Physicians delineated key structures, including the iGTV, CTV, trachea, and thoracic vertebrae, in two sets of CT scans obtained around the 20-min mark. After aligning the two images, changes in the anatomical structures were quantitatively assessed using the Dice similarity coefficient (DSC) [35]. The DSC formula is as follows:

$$DSC = \frac{2|A \cap B|}{|A| + |B|} \quad (1)$$

Here A represents the volume of anatomical structures immediately before, and B represents the volume of anatomical structures 20 min later. This approach is a robust method for evaluating the dynamic stability of anatomical structures during treatment. When $DSC = 1$, this signifies a complete overlap between the two structures. In addition to assessing the settling of patient anatomical structures during the inclined period, the patient's intra-fractional movement and iso-rotational accuracy of pod rotation should also be evaluated. In the alignment process described above, the difference between PE-B1 and PE-B2 represents the entire positioning error involving the POD movement, IGRT system, and patient intrafraction movement [1].

Statistical significance was assessed using a two-tailed paired Student's t -test; $p < 0.05$ was considered statistically significant.

The Institutional Review Board reviewed and approved this study.

3 Results

3.1 Pre-dosimetry study

The volumes of the iGTV receiving more than 99% of the prescription dose (V99) were $99.9\% \pm 0.3\%$ (median \pm standard deviation) for the pod plans and $99.9\% \pm 0.8\%$ for the couch plans, and $p = 0.15$ indicates no significant difference. The average dose to the lung-iGTV in the pod plans for the 11 patients decreased by 5–53%, with a p -value less than 0.01 compared to that of the plans using the treatment couch (Fig. 2). Moreover, no significant differences were observed in other OARs, such as the heart, esophagus, spinal cord, and trachea.

3.2 Planning and dosimetric comparison

For all seven patients, both the pod and supine plans had comparable target coverage. The V99 of the iGTV for the pod plans were $99.8\% \pm 7.4\%$ and $99.9\% \pm 3.7\%$ for the supine plans; $p = 0.31$ indicates no significant difference. The V99 of the CTV for the pod plans were $98.8\% \pm 8.3\%$ and $99.9\% \pm 8.4\%$ for the supine plans; $p = 0.19$ indicates no significant difference. Except for the mean dose to the lung-iGTV, there were no significant differences in the other OARs between the pod and supine plans. The detailed data on the targets and OARs are presented in Table 2. The mean dose to the lung-iGTV is shown in Fig. 3. Notably, for patients numbered 3–6, the dose to the lungs was significantly reduced in the pod plan. While the remaining three patients showed no significant difference in the lung dose, the utilization of the 90° beamline in their cases resulted in a substantial reduction in the patient admission waiting time.

3.3 Patient alignment

The median treatment duration (from entering to exiting the pod) for the seven patients treated with the pod was 35 min

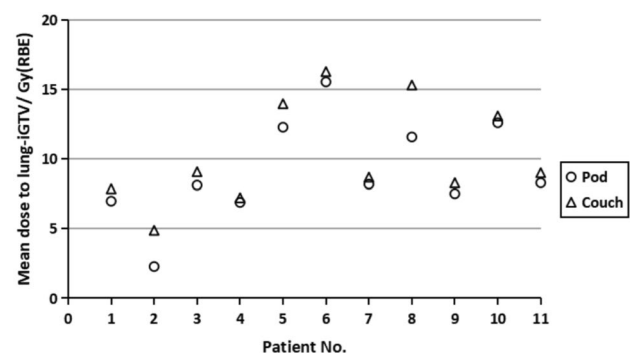
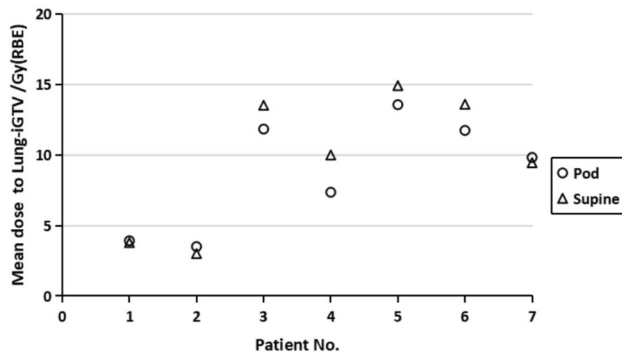
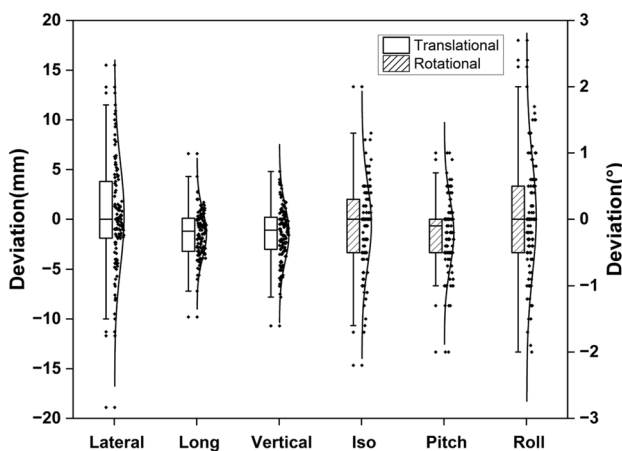
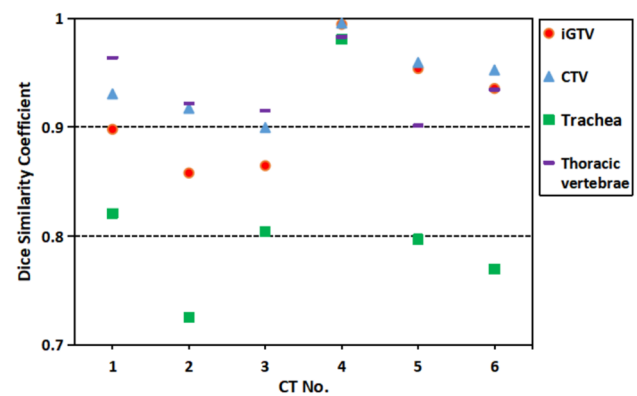


Fig. 2 The mean dose to lung-iGTV of pod plans and couch plans

Table 2 Comparisons of organs at risk of the pod and supine plans

ROI	Parameter	Pod plan	Supine plan	<i>p</i> value
iGTV	V99 (%)	99.8 ± 7.4	99.9 ± 3.7	0.31
CTV	V99 (%)	98.8 ± 8.3	99.9 ± 8.4	0.19
Lung-iGTV	D_{mean} [Gy(RBE)]	9.8 ± 3.7	10.0 ± 4.4	0.04
Lung-iGTV	V5 (%)	22.4 ± 10.3	28.2 ± 11.5	0.04
Lung-iGTV	V20 (%)	15.8 ± 6.3	15.4 ± 8.4	0.09
Heart	D_{mean} [Gy(RBE)]	4.6 ± 3.5	5.9 ± 3.5	0.83
Spinal cord	D_{max} [Gy(RBE)]	25.7 ± 13.1	28.2 ± 16.5	0.48
Trachea	D_{max} [Gy(RBE)]	78.8 ± 26.8	78.0 ± 19.3	0.72
Esophagus	D_{max} [Gy(RBE)]	78.4 ± 31.5	78.4 ± 34.1	0.50
Esophagus	D_{mean} [Gy(RBE)]	13.2 ± 10.6	17.92 ± 17.0	0.09

**Fig. 3** Mean dose to the lung-iGTV of the pod and supine plans**Fig. 4** Positional error between beams for all fractions. The left y-axis corresponds to the translational deviations (mm), and the right y-axis corresponds to rotational deviations (°). The boxes represent the interquartile range, with the median line inside each box. Whiskers extend to 1.5 times the interquartile range, and outliers are depicted as individual points**Fig. 5** Color online Dice similarity coefficient for different anatomical structures for 20-min intervals

(SD 14 min) per fraction. The positional errors between the beams were recorded and calculated. Figure 4 depicts the deviations in the six directions for all seven patients. The median deviations for the lateral, longitudinal, vertical, ISO, pitch, and roll directions are $0.0 \text{ mm} \pm 5.3 \text{ mm}$, $-1.2 \text{ mm} \pm 2.3 \text{ mm}$, $-1.1 \text{ mm} \pm 2.7 \text{ mm}$, $0.0^\circ \pm 0.6^\circ$, $-0.1^\circ \pm 0.5^\circ$, and $0.0^\circ \pm 0.8^\circ$, respectively.

For each fraction, the deviation frequencies in the lateral, longitudinal, and vertical directions within 5 mm were 72%, 95%, and 88%, respectively. For deviations within 10 mm, the frequencies were 93%, 100%, and 99% in the three translational directions, respectively. In the iso, pitch, and roll directions, 91%, 96%, and 87% of the deviations were within 1° , respectively. No deviations exceeding 2° were observed for any of the rotational axes. Notably, these deviations were recorded prior to applying the position correction before the second beam delivery, indicating that they did not affect the precision of the treatment.

4 Position accuracy analysis

Six pairs of CT images were acquired. The DSC for the iGTV, CTV, trachea, and thoracic vertebrae based on CT images acquired 20-min apart was calculated and recorded.

As shown in Fig. 5, the tumor target and thoracic vertebrae exhibited a high DSC, indicating good stability of these structures. However, the trachea showed a DSC value of approximately 0.8, suggesting potential settling after 20 min of rotation. Nevertheless, a 1–2 mm planning organ-at-risk volume will be expanded during planning, ensuring that its dose remains within safe limits.

5 Discussion

In this study, we illustrated the efficacy of the pod in achieving target coverage while minimizing doses to OARs and highlighted the challenges associated with treating lung tumors using a rotational pod. Additionally, we presented patient data from a clinical trial and analyzed the position accuracy and stability of anatomical structures.

The pod's capability to simulate the impact of a rotational gantry provides a pragmatic remedy for institutions that lack access to carbon-ion rotational gantries. The study revealed a notable reduction in the lung dose in four of the seven patients, suggesting a potential advantage in mitigating radiation exposure to healthy tissues. A lower mean lung dose effectively reduced the risk of radiation pneumonitis [36]. While the remaining three patients did not show dosimetric benefits with the pod plans, the shorter admission waiting time associated with the pod plans aligns with patient-centric considerations. A reduced waiting period for admission may additionally attenuate tumor growth during this interval and diminish the likelihood of treatment replanning.

Patient intra-fractional movements and the rotational accuracy of the robotic arm were the main contributors to the differences between PE-B1 and PE-B2. Sheng et al. validated the submillimeter mechanical accuracy of a robotic arm in our facility [2]. We observed millimeter-level inter-beam movements, with 5–28% of the beams experiencing translational shifts exceeding 5 mm. In Lu's study, 46.7% of the patients exhibited intra-fractional movements exceeding 3 mm [37]. Zhong et al. reported the presence of 5 mm-level systematic and random errors in lung cancer [38]. These results are consistent with the data presented in the present study. This could be attributed to the presence of millimeter-scale motion spaces in patients, even when thermoplastic masks are in place. In addition, the patient's respiratory and cardiac motions contributed to this error. However, it is worth noting that Fig. 4 indicates that the error follows a Gaussian distribution, with 72–95% of the data in the three translational directions falling within 5 mm. Although individual fractions exceeding 5 mm can lead to underdosing of the target or overdosing of OARs, segmentation into 10–22 fractions can reduce the impact of single-fraction errors to some extent. In addition, this millimeter-level inter-beam movement suggests the possibility of relative displacement between the patient, pod, and foam. However, because the pod is designed to be uniform in water equivalence at all angles and depths, and the foam is a low-density material, this error theoretically has a minimal impact on dosimetry. Kanai et al. examined the dosimetric effects of

displacement between the patient and the treatment couch when a carbon-ion beam passed through the couch using a rotating gantry. For patients with lung cancer, an average displacement of 4.2 mm was observed; however, dosimetric analysis indicated no significant impact on the target coverage and V20 of the ipsilateral lung [39]. Based on these potential effects, a 7–15 mm margin was expanded to generate the PTV during treatment planning. In addition, position verification at each iso-rotation angle is strongly recommended to eliminate this error and ensure accuracy.

The time required for pod treatment is $35 \text{ min} \pm 14 \text{ min}$ per fraction, while the treatment couch, also for lung cancer patients, requires $21.5 \text{ min} \pm 4 \text{ min}$. As described earlier, the difference between PE-B1 and PE-B2 can sometimes exceed 5 mm, which necessitates position verification before each beam irradiation. This additional step extends the treatment time. However, from the perspective of beamline efficiency, this has a minimal impact because our facility is equipped with four treatment rooms. During position verification, the beamline can be allocated to other rooms, and the treatment can proceed once position correction is completed. Therefore, there was no significant difference in the beam time between the pod patients and those using the treatment couch.

To the best of our knowledge, there is a lack of clinical data on the settling effects of organs when patients shift from an upright to a lying-down or tilted position. Importantly, this settling phenomenon is not confined to patients undergoing pod treatment; individuals in the supine or prone positions, transitioning from a standing to a lying-down posture, may also experience potential settling of internal body structures. In this study, DSC was used to evaluate the settling of the tumors, trachea, and vertebrae 20 min after the patients underwent a specific rotational angle. The DSC of these structures, excluding the trachea, was found to be greater than 0.85, which is considered an appropriate threshold for automatic image segmentation [40].

The pod, as a gantry-free solution, can provide more freedom in beam-angle selection when used with a fixed ion beamline compared to the fixed beamline itself. Although it can simulate a 360-degree beam angle, patient stability may be a concern. Although its impact is small, the use of a rotating gantry eliminates the issue of patient stability. We acknowledge this as a disadvantage compared to the gantry. Nevertheless, its low cost makes it a viable option for low- and middle-income countries. The recent trend in upright radiotherapy, facilitated by chairs that can rotate 360 degrees, provides an alternative to rotational gantries [22, 41, 42]. However, this approach is only suitable for treating patients with head and neck lesions in the absence of an upright CT [1]. One notable advantage of the pod is that it eliminates the need for an additional

upright CT, distinguishing it from the limitations associated with the current trend of upright radiotherapy. This study has certain limitations, such as a relatively small sample size. However, in the developmental phase of an innovation, studies with small sample sizes can play a pivotal role, and further investigation is required on this topic. Additionally, owing to the lack of real-time KV imaging guidance, it was not possible to obtain patient movement data within individual treatment fields for the analysis and mitigation of patient motion. Further research and technological advancements are required to refine and expand the clinical applications of rotating pods in radiation therapy.

6 Conclusion

Preliminary clinical application of the rotational pod for lung tumor in fixed ion beamlines presents promising results. This study provides clinical data on the dosimetric considerations, treatment efficiency, and anatomical structural stability associated with rotational pod treatment. However, as an innovative solution to the challenges of ion beam therapy, the rotating pod at SPHIC warrants further exploration and refinement. Future developments could focus on enhancing patient comfort by introducing 3D printing into patient immobilization procedures and establishing robust simulation systems with 4D optimization to further refine treatment plans. Continued research and clinical trials, including those expanding the indications for breast cancer and other malignancies, are essential for validating and optimizing the efficacy of this novel approach.

Acknowledgements The authors appreciate Michael F. Moyers from the Shanghai Proton and Heavy Ion Center for designing the rotational pods.

Author contributions All authors contributed to the study conception and design. Material preparation, data collection, and analysis were performed by Jia-Yao Sun, Wen-Xuan Yang, Ya-Qi Li, Jian Chen, Jing-Fang Mao, Ning-Yi Ma, Yin-Xiang-Zi Sheng, Wei-Wei Wang, Dan You, and Kai-Liang Wu. The first draft of the manuscript was written by Jia-Yao Sun and Wen-Xuan Yang, and all authors commented on the previous versions of the manuscript. All authors read and approved the final manuscript.

Data availability The data that support the findings of this study are openly available in Science Data Bank at <https://cstr.cn/31253.11.sciencedb.j00186.00556> and <https://www.doi.org/10.57760/sciencedb.j00186.00556>.

Declarations

Conflict of interest The authors declare that they have no conflict of interest.

References

1. J. Sun, L. Kong, Z. Chen et al., Clinical implementation of a 6D treatment chair for fixed ion beam lines. *Front. Oncol.* **11**, 694749 (2021). <https://doi.org/10.3389/fonc.2021.694749>
2. Y. Sheng, J. Sun, W. Wang et al., Performance of a 6D treatment chair for patient positioning in an upright posture for fixed ion beam lines. *Front. Oncol.* **10**, 122 (2020). <https://doi.org/10.3389/fonc.2020.00122>
3. S. Mori, Y. Sakata, R. Hirai et al., Commissioning of a fluoroscopic-based real-time markerless tumor tracking system in a superconducting rotating gantry for carbon-ion pencil beam scanning treatment. *Med. Phys.* **46**(4), 1561 (2019). <https://doi.org/10.1002/mp.13403>
4. N. Kanematsu, T. Furukawa, Y. Hara et al., New technologies for carbon-ion radiotherapy - developments at the National Institute of Radiological Sciences, QST. *Japan. Radiat. Phys. Chem.* **162**, 90 (2019). <https://doi.org/10.1016/j.radphyschem.2019.04.038>
5. Y. Iwata, T. Fujimoto, S. Matsuba et al., Beam commissioning of a superconducting rotating-gantry for carbon-ion radiotherapy. *Nucl. Instrum. Meth. Phys. Res. Sect. A* **834**, 71–80 (2016)
6. T. Bhattacharyya, M. Koto, H. Ikawa et al., First prospective feasibility study of carbon-ion radiotherapy using compact superconducting rotating gantry. *Br. J. Radiol.* **92**, 1103 (2019). <https://doi.org/10.1259/bjr.20190370>
7. U. Weinrich. Gantry design for proton and carbon hadrontherapy facilities. In: 10th European Particle Accelerator Conference (EPAC 06), 964–968 (2006)
8. S. Takayama, T. Yazawa, M. Asano et al., Design and magnetic field measurement of the superconducting magnets for the next-generation rotating gantry. *IEEE. Trans. Appl. Supercond.* **32**(6), 1–4 (2022). <https://doi.org/10.1109/TASC.2022.3160973>
9. Y. Luo, S. Huang, H. Zhang et al., Assessment of the induced radioactivity in the treatment room of the heavy-ion medical machine in Wuwei using PHITS. *Nucl. Sci. Tech.* **34**, 29 (2023). <https://doi.org/10.1007/s41365-023-01181-8>
10. S. Huang, H. Zhang, K. Bai et al., Monte Carlo study of the neutron ambient dose equivalent at the heavy ion medical machine in Wuwei. *Nucl. Sci. Tech.* **33**, 119 (2022). <https://doi.org/10.1007/s41365-022-01093-z>
11. Q. Li, L. Sihver, Therapeutic techniques applied in the heavy-ion therapy at IMP. *Nucl. Instrum. Meth. Phys. B* **269**(7), 664–670 (2011). <https://doi.org/10.1016/j.nimb.2011.01.125>
12. J.L. Wang, L. Cruz, Q. Wu et al., Radiation shielding design of a compact single-room proton therapy based on synchrotron. *Nucl. Sci. Tech.* **31**, 1 (2019). <https://doi.org/10.1007/s41365-019-0712-1>
13. Y. Li, X. Li, J. Yang et al., Flourish of proton and carbon ion radiotherapy in China. *Front. Oncol.* **12**, 819905 (2022). <https://doi.org/10.3389/fonc.2022.819905>
14. J. Sun, Z. Wang, Y. Sheng et al., Indications of IMRT, PRT and CIRT for HCC from comparisons of dosimetry and normal tissue complication possibility. *Strahlenther. Onkol.* **198**, 361–369 (2022). <https://doi.org/10.1007/s00066-021-01854-6>
15. J. Chen, J.J. Lu, N. Ma et al., Early stage non-small cell lung cancer treated with pencil beam scanning particle therapy: retrospective analysis of early results on safety and efficacy. *Radiat. Oncol.* **14**(1), 16 (2019). <https://doi.org/10.1186/s13014-019-1216-1>
16. S. Liang, G. Zhou, W. Hu, Research progress of heavy ion radiotherapy for non-small-cell lung cancer. *Int. J. Mol. Sci.* **23**, 4 (2022). <https://doi.org/10.3390/ijms23042316>
17. M. Nakajima, N. Yamamoto, K. Hayashi et al., Carbon-ion radiotherapy for non-small cell lung cancer with interstitial lung disease: a retrospective analysis. *Radiat. Oncol.* **12**(1), 144 (2017). <https://doi.org/10.1186/s13014-017-0881-1>

18. R. Baker, G. Han, S. Sarangkasiri et al., Clinical and dosimetric predictors of radiation pneumonitis in a large series of patients treated with stereotactic body radiation therapy to the lung. *Int. J. Radiat. Oncol. Biol. Phys.* **85**(1), 190 (2013). <https://doi.org/10.1016/j.ijrobp.2012.03.041>
19. J. Timmeren, S. Ehrbar, M. Chamberlain, Single-isocenter versus multiple-isocenters for multiple lung metastases: evaluation of lung dose. *Radiother. Oncol.* **166**, 189 (2022). <https://doi.org/10.1016/j.radonc.2021.11.030>
20. L. Hoffmann, M. Knap, M. Alber et al., Optimal beam angle selection and knowledge-based planning significantly reduces radiotherapy dose to organs at risk for lung cancer patients. *Acta. Oncol.* **60**(3), 293 (2021). <https://doi.org/10.1080/0284186X.2020.1856409>
21. X. Zhang, W. Hsi, F. Yang et al., Development of an isocentric rotating chair positioner to treat patients of head and neck cancer at upright seated position with multiple nonplanar fields in a fixed carbon-ion beamline. *Med. Phys.* **47**(6), 2450 (2020). <https://doi.org/10.1002/mp.14115>
22. L. Volz, Y. Sheng, M. Durant et al., Considerations for upright particle therapy patient positioning and associated image guidance. *Front. Oncol.* **12**, 930850 (2022). <https://doi.org/10.3389/fonc.2022.930850>
23. C. Essen, H. Blattmann, J. Crawford et al., The PIOTRON: initial performance, preparation and experience with pion therapy. *Int. J. Radiat. Oncol. Biol. Phys.* **8**(9), 1499 (1982). [https://doi.org/10.1016/0360-3016\(82\)90609-5](https://doi.org/10.1016/0360-3016(82)90609-5)
24. M. Moyers, LLUPTF: eleven years and beyond. *AIP Conf. Proceed.* **610**, 305–309 (2002). <https://doi.org/10.1063/1.1469940>
25. H. Tsujii, J. Mizoe, T. Kamada et al., Overview of clinical experiences on carbon ion radiotherapy at NIRS. *Radiother. Oncol.* **73**(Suppl 2), S41 (2004). [https://doi.org/10.1016/s0167-8140\(04\)80012-4](https://doi.org/10.1016/s0167-8140(04)80012-4)
26. P. Liu, R. O'Brien, S. Heng et al., Development and commissioning of a full-size prototype fixed-beam radiotherapy system with horizontal patient rotation. *Med. Phys.* **46**(3), 1331 (2019). <https://doi.org/10.1002/mp.13356>
27. W. Takahashi, S. Mori, M. Nakajima et al., Carbon-ion scanning lung treatment planning with respiratory-gated phase-controlled rescanning: simulation study using 4-dimensional CT data. *Radiat. Oncol.* **9**, 238 (2014). <https://doi.org/10.1186/s13014-014-0238-y>
28. J. Chen, J. Mao, N. Ma et al., Definitive carbon ion radiotherapy for tracheobronchial adenoid cystic carcinoma: a preliminary report. *BMC. Cancer.* **21**(1), 734 (2021). <https://doi.org/10.1186/s12885-021-08493-1>
29. N. Ma, J. Chen, X. Ming et al., Preliminary safety and efficacy of proton plus carbon-ion radiotherapy with concurrent chemotherapy in limited-stage small cell lung cancer. *Front. Oncol.* **11**, 766822 (2021). <https://doi.org/10.3389/fonc.2021.766822>
30. X. Li, C. Stepaniak, E. Gore, Technical and dosimetric aspects of respiratory gating using a pressure-sensor motion monitoring system. *Med. Phys.* **33**(1), 145 (2006). <https://doi.org/10.1118/1.2147743>
31. T. Elsasser, M. Kramer, M. Scholz, Accuracy of the local effect model for the prediction of biologic effects of carbon ion beams in vitro and in vivo. *Int. J. Radiat. Oncol. Biol. Phys.* **71**(3), 866 (2008). <https://doi.org/10.1016/j.ijrobp.2008.02.037>
32. W. Wang, Y. Ma, H. Zhang et al., Comparison between 4D robust optimization methods for carbon-ion treatment planning. *Nucl. Sci. Tech.* **34**, 139 (2023). <https://doi.org/10.1007/s41365-023-01285-1>
33. S. Jia, J. Chen, N. Ma et al., Adaptive carbon ion radiotherapy for locally advanced non-small cell lung cancer: organ-sparing potential and target coverage. *Med. Phys.* **49**(6), 3980 (2022). <https://doi.org/10.1002/mp.15563>
34. N. Ma, X. Ming, J. Chen et al., Dosimetric rationale and preliminary experience in proton plus carbon-ion radiotherapy for esophageal carcinoma: a retrospective analysis. *Radiat. Oncol.* **18**(1), 195 (2023). <https://doi.org/10.1186/s13014-023-02371-9>
35. J. You, Q. Wang, R. Wang et al., Deep learning-aided automatic contouring of clinical target volumes for radiotherapy in breast cancer after modified radical mastectomy. *Front. Phys.* **9**, 754248 (2022). <https://doi.org/10.3389/fphy.2021.754248>
36. A. Niezink, A. Schaaf, R. Wijsman et al., External validation of NTCP-models for radiation pneumonitis in lung cancer patients treated with chemoradiotherapy. *Radiother. Oncol.* **186**, 109735 (2023). <https://doi.org/10.1016/j.radonc.2023.109735>
37. L. Lu, C. Diaconu, T. Djemil et al., Intra- and inter-fractional liver and lung tumor motions treated with SBRT under active breathing control. *J. Appl. Clin. Med. Phys.* **19**(1), 39 (2018). <https://doi.org/10.1002/acm2.12220>
38. R. Zhong, J. Wang, L. Zhou et al., Implementation of single-breath-hold cone beam CT guided hypofraction radiotherapy for lung cancer. *Radiat. Oncol.* **9**, 77 (2014). <https://doi.org/10.1186/1748-717X-9-77>
39. T. Kanai, W. Furuichi, S. Mori, Evaluation of patient positional reproducibility on the treatment couch and its impact on dose distribution using rotating gantry system in scanned carbon-ion beam therapy. *Phys. Med.* **57**, 160–168 (2019). <https://doi.org/10.1016/j.ejmp.2018.12.013>
40. G. Loi, M. Fusella, E. Lanzi et al., Performance of commercially available deformable image registration platforms for contour propagation using patient-based computational phantoms: A multi-institutional study. *Med. Phys.* **45**(2), 748 (2018). <https://doi.org/10.1002/mp.12737>
41. S. Boissbouvier, T. Underwood, J. McNamara et al., Upright patient positioning for gantry-free breast radiotherapy: feasibility tests using a robotic chair and specialised bras. *Front. Oncol.* **13**, 1250678 (2023). <https://doi.org/10.3389/fonc.2023.1250678>
42. J. Marano, M. Kissick, T. Underwood et al., Relative thoracic changes from supine to upright patient position: a proton collaborative group study. *J. Appl. Clin. Med. Phys.* **24**(12), e14129 (2023). <https://doi.org/10.1002/acm2.14129>

Springer Nature or its licensor (e.g. a society or other partner) holds exclusive rights to this article under a publishing agreement with the author(s) or other rightsholder(s); author self-archiving of the accepted manuscript version of this article is solely governed by the terms of such publishing agreement and applicable law.